PCCP

ROYAL SOCIETY OF CHEMISTRY

PAPER

View Article Online
View Journal | View Issue

Cite this: *Phys. Chem. Chem. Phys.*, 2020, **22**, 13764

SAXS signature of the lamellar ordering of ionic domains of perfluorinated sulfonic-acid ionomers by electric and magnetic field-assisted casting†

Jaqueline S. da Silva,[a] Sabrina G. M. Carvalho,[a] Rodrigo P. da Silva,[a] Ana C. Tavares,[b] Ulrich Schade,[c] Ljiljana Puskar,[c] Fabio C. Fonseca[a] and Bruno R. Matos*[a]

Received 6th April 2020,
Accepted 5th June 2020

DOI: 10.1039/d0cp01864c

rsc.li/pccp

At present, small angle X-ray scattering (SAXS) studies of perfluorinated sulfonic-acid ionomers (PFSAs) are unable to fully determine the true shape of their building blocks, as recent SAXS modelling predicts disk- and rod-like nanoionic domains as being equally possible. This scenario requires evidence-based findings to unravel the real shape of PFSA building blocks. Herein, a SAXS pattern signature for a lamellar nanophase separation of the ionic domains of Nafion is presented, backed by mid and far infrared spectroscopy (MIR and FIR) and wide angle X-ray scattering (WAXS) data of Nafion in different ionic forms, a broad range of ionic phase contents (EW ∼ 859–42 252 g eq^{-1}) and temperatures. The study indicates that the lamellar arrangement of the ionic domains is the most representative morphology that accounts for the physical properties of this ionomer. The lamellar SAXS reflections of Nafion are enhanced in electric and magnetic field-aligned membranes, as confirmed by atomic force microscopy (AFM). Electric and magnetic field-assisted casting of Nafion allowed producing nanostructured and anisotropic films with the lamellas stacked perpendicularly to the field vector, which is the direction of interest for several applications. Such nanostructured Nafion membranes are bestowed with advanced optical and proton transport properties, making them promising materials for solar and fuel cells.

1. Introduction

As a benchmark electrolyte in proton exchange membrane fuel cells (PEM), the outstanding properties of perfluorinated sulfonic-acid ionomers (PFSAs), such as anisotropic water transport, thin-film confinement, giant dielectric permittivity, humidity enhanced mechanical properties, memory of shape and electromechanical actuation, have projected PFSAs towards several remarkable applications such as artificial muscle design, supercapacitors, 4D printing and electric-driven displays.[1,2] In order to predict the final physical properties of PFSAs, it is of great importance to master the relation between the dynamics of the ionic network and the shape of the building block, which is still a limiting step and therefore a matter of intense research.[1–3]

There is an ever increasing list of PFSA membranes, such as Nafion (Dupont), Flemion (Asahi Glass), Aciplex (Asahi Kasei), Dow (Dow Chemicals), 3M (3M) and Aquivion/Hyflon (Solvay Solexis), with modified length and composition of the main and side chains in order to alter the state of aggregation of ions and promote an improvement of their proton conduction properties.[1] However, Nafion membranes are considered a reference PFSA since most of the characterizations have concentrated on this ionomer.

As a complicating factor, the commercial Nafion films, prepared by extrusion, are converted to the ionic form after the film is formed, which increases the complexity of cracking the ionomer morphology by the following reason: the ionic clusters are formed within the non-ionic polymer structure with an already existing phase separation of the perfluorinated backbone and side chains.[1] Interestingly, Nafion membranes prepared by casting exhibit a very similar phase separation of the ionic and non-ionic domains to that of the extruded films, as confirmed by the similar features of both ionomer and matrix peaks in the SAXS plots.[1,4] Therefore, the study of membranes prepared by casting served as the basis for elucidating many aspects of the ionic and non-ionic aggregation in Nafion.[1,4] By an investigation of the structural evolution from the Nafion films

[a] *Instituto de Pesquisas Energéticas e Nucleares, IPEN-CNEN/SP, São Paulo 05508000, Brazil. E-mail: brmatos@usp.br*
[b] *Énergie, Matériaux et Télécommunications (INRS-EMT), Institut National de la Recherche Scientifique, 1650 Boulevard Lionel-Boulet, Varennes, Québec, J3X 1S2, Canada*
[c] *Methoden der Materialentwicklung, Helmholtz-Zentrum für Materialien und Energie GmbH, Berlin, 12489, Germany*

† Electronic supplementary information (ESI) available. See DOI: 10.1039/d0cp01864c

to solutions, Gebel *et al.* provided the most reliable semi-phenomenological model of PFSAs, mostly based on small angle X-ray scattering (SAXS), NMR spectroscopy, atomic force (AFM) and transmission electron (TEM) microscopies.[4,5] The building blocks of Nafion solutions were shown to be composed of crystalline and amorphous phases in the shape of elongated and micellar polymeric aggregates with a radius of $r \sim 2.5$–4 nm and length $L > 100$ nm.[4,5] Such phenomenological model provided strong empirical findings for a concise mathematical evaluation of SAXS patterns of Nafion membranes, which allowed a deeper understanding of the relation between microstructure and macroscopic properties.[2] Such SAXS model of Nafion is currently the most accepted morphology for the building blocks of PFSAs, which is described as a parallel packing of nearly cylindrical inverted-micelle polymeric aggregates forming a bunch of aligned cylinders at short length scales, isotropically displaced within the ionomer matrix in a macroscopic level.[2] However, a critical evaluation of the previous SAXS theoretical modelling of Nafion evidenced that the shape of the nanophase separation of ionic and non-ionic domains could be predicted as having either rod- or disk-like domains, revealing a demand for new experimental data that can unequivocally determine the real shape of Nafion building blocks.[6,7] Considering both the inverted micellar cylindrical geometry and the water sorption capacity for Nafion, the large water volume fraction absorbed by the film and the high concentration of the protonic charges in the cylindrical core would promote a thermodynamically unstable morphology, as intense electrostatic repulsion would exist among nanoconfined dissociated protons.[6] On the other hand, it is predicted that the electrostatic interactions existing within locally flat or lamellar ionic phase are stabilized by thin disk-like water domains that act as a "glue" holding the nanostructure together.[6,8] In fact, in several reports, the lamellar arrangement of the ionic domains in Nafion has been inferred or at least suggested.[6,7,9–11,46,59] In this scenario, the SAXS modelling of PFSAs lacks evidence-based findings to be used as pivot data for the convergence of a more plausible mathematical/phenomenological model of Nafion. One of the main setbacks in advancing this structural understanding resides on the insufficient information of the representative monomeric sequence of PFSAs.[1]

Nafion is a statistical copolymer created by a free radical copolymerization reaction of tetrafluoroethylene (TFE) monomer with a perfluorovinyl ether side group comonomer, as shown in Fig. 1.[1]

The m is 6–7 for Nafion membranes with equivalent weight (EW) of 1100 g eq^{-1} representing an average separation among neighbouring side chains of 14 CF_2 units.[1] Often for the sake of simplicity, in mathematical/phenomenological models of Nafion, the monomeric sequence distribution is described as either random or ideally spaced (as indicated by the chemical formula) by the chemical formula.[1] Previous simulation studies of the ionic clustering of Nafion considered two possible extreme cases for its chemical structure, one dispersed—with the side chains regularly spaced between 14 CF_2 units—and one concentrated comb-coil diblock—with side chains grouped along with 70 CF_2 units.[9] The results showed that the phase separation into ionic and non-ionic domains is favoured with increasing blockiness of the polymeric backbone.[9] In other types of copolymer systems, for example, the SAXS measurements of sulfonated copolymers, such as poly(arylene ether sulfone), with a well-characterized random monomeric distribution of the ionic groups revealed that the ionomer peak is absent.[10–12] Strong empirical facts, such as the large crystallite size and the long persistence length, point out that the effective monomer/comonomer distribution of Nafion chains cannot be considered aleatory or ideally regular.[9,13,14] Since the side chains cannot be accommodated in well-ordered crystalline domains, the typically observed crystallite size of 4.4 nm of Nafion estimated by X-ray diffraction, indicates a sequence of 34 CF_2 units.[13] Similarly, long persistence lengths (10–40 nm) estimated by AFM for Nafion single chains in aqueous solution, suggest that the electrostatic repulsions among short spaced side chains affect the contour length of the backbone.[2,14]

Furthermore, in a regular distribution ($m = 7$), the distance between two neighbouring side chains in Nafion is 19 Å on average, and in the blocky distribution such distance can reach values lower (5 Å) than the Bjerrum length ($l_b = 7$ Å) resulting in a critical linear charge density in the segments rich in side chains $\{n = zl_b/h > 1$, where h is the separation of monovalent charges $(z)\}$.[9,15] Therefore, a high linear density of side chains in the polymer backbone of Nafion would promote the condensation of counterions in the sulfonic acid groups in order to minimize electrostatic repulsion.[15] As ionomer materials are known to contain a low molar fraction of ionic groups, if the spacing among side chains is considered to be longer than the Bjerrum length, the sulfonic groups would have a higher degree of freedom for minimizing the repulsive forces, thereby escaping from the counterion condensation phenomena. However, fluorescence spectroscopy and SAXS measurements for samples in equilibrium with different pH confirmed the existence of condensed counterions in Nafion.[16,17] The existence of counterion condensation suggests that backbone segments rich in side chains are possibly an intrinsic feature of Nafion chemical structure. The investigations of ^{19}F and ^{13}C NMR resonances of Nafion identified the existence of long runs of TFE in the backbone, but the exact monomeric sequence number could not be estimated with precision.[18,19] Other NMR studies reported that the pendant side groups are aggregated into ~3.8 nm domains with a periodicity of ~10 nm.[20] As a consequence, the determination of the representative distribution of the main and side chains along the backbone would refine the morphological modelling and solve important open questions regarding

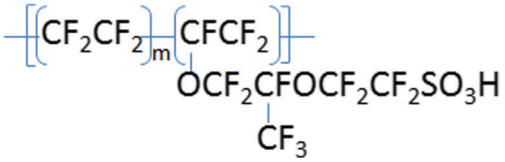

Fig. 1 Chemical structure of Nafion: m represents the relative sequence of TFE and the side groups along the main chain.

the physical properties of Nafion such as the giant dielectric permittivity, Donnan exclusion effects, and water sorption capacity.[21–24]

A promising strategy for revealing the underlying morphology of PFSA is by increasing the ordering of the ionic domains. This can be achieved by thermal annealing thus promoting thermal transitions of higher ordering,[1] by the replacement of protons with alkali counterions which increases the electrostatic dipolar attractions among sulfonic groups,[1] or by producing films under electric and magnetic fields.[25–29] The preparation of PFSA films with the use of electric-assisted casting has been incipiently explored.[27,28] Previous reports showed that the microstructure of Nafion films can be aligned by electric field-assisted casting, revealing an improvement of the proton conduction properties.[27,28] Increased structure anisotropy and proton conductivity of films produced with such a method are of great interest for many electrochemical applications.[1] However, a detailed SAXS study that would indicate the main orientations of the internal structure is still missing for aligned PFSA.[27,28] Another interesting aspect in the structural alignment of Nafion films is the extremely low electric field values employed.[28] The structure of Nafion revealed to be liable to the alignment under electric fields of the order of $\sim 10^1$ V cm^{-1}, whereas for many block copolymers the effective alignment is only observed for electric fields higher than $\sim 10^3$ V cm^{-1}.[27] The facile structuring of Nafion films casts doubts on the polarizability mechanism of the building blocks, which is also a topic related to the distribution of the side chains along the polymer backbone. Similarly, the use of magnetic field-assisted casting is rarely explored for ionomers and to the best of our knowledge, not found for PFSA. Some studies reported that magnetic field nanostructured composite membranes using ferrocyanide coordinated polymers or iron-based nanoparticles exhibited a high through-plane conductivity.[25,26] However, the magnetic-field alignment of pure polymer materials has been greatly advanced allowing the production of highly ordered polymer films without resorting to iron-based systems.[29]

Herein, the strategy of increasing the ordering of both ionic and non-ionic domains was employed in order to enhance the contrast among the distinct phases in Nafion. Specifically, a higher ordering of the non-ionic domains of Nafion was achieved by thermal annealing above the α-transition temperature; the ordering of the ionic domains was obtained by changing the ionic phase content (and ionic form), by preparing Nafion membranes with different weight (EW)—in an EW range not yet explored; and finally, highly ordered ionic domains were obtained by preparing Nafion films using electric and magnetic field-assisted casting. SAXS, WAXS, AFM and Fourier-transform infrared (FTIR) spectroscopy were combined in order to assess the relation between microstructure and electrostatic interactions as well as the existing trade-off between the ordering/disordering in both ionic and non-ionic phases. The ordering/disordering of the non-ionic phase points out to a necessary revision of the origin of the matrix peak in Nafion SAXS plots. Moreover, with the use of such techniques, it was possible to identify in highly ordered Nafion films, anisotropic patterns of the intense lamellar reflections, confirming an empirical signature for the lamellar ordering of the ionic domains. Such nanostructured Nafion membranes display a preferential orientation of the lamellar planes of the ionic phase in the perpendicular direction with respect to both electric and magnetic fields, which resulted in enhanced electrochemical and optical properties.

2. Experimental

2.1. Nafion Materials

Commercial Nafion membranes (EW = 1100 g eq^{-1}) were obtained from DuPont with different thicknesses (N112/N115/N117). Nafion pellets (Ion Power) in the non-ionic form (RSO_2F, EW = 1000 g eq^{-1}) were used to prepare 100 μm films by hot-pressure. Commercial Nafion 5% solutions (DuPont) were used to prepare the membranes by casting.

2.2. Materials preparation

2.2.1. Thermal annealing procedure. The nanophase separation in Nafion undergoes strong modifications when the sample is heated above the glass and α-transitions.[1] The thermal annealing was carried out *in situ* for SAXS/WAXS and for mid and far infrared measurements. With the former, information regarding the phase structural shapes was obtained, which could be compared with the state of the electrostatic interactions, as inferred from the latter FTIR data. The details of the equipment and parameters for the thermal annealing are provided in the specific sections for each technique.

2.2.2. Nafion membranes with different equivalent weight. Nafion pellets in the non-ionic form (RSO_2F − EW = 1000 g eq^{-1}) were hot-pressed above the polymer melting temperature (220 °C) within a Teflon mask for reaching the thickness of 100 μm. These films were quenched in liquid N_2 to minimize TFE recrystallization. These films were converted to SO_3Na groups by nucleophilic substitution using the DuPont standard conversion procedure. By immersing the films in NaOH solutions in H_2O/DMSO at 60 °C for 6 h, and by varying the concentration from 1.1×10^{-4} g mL^{-1} to 3.2×10^{-1} g mL^{-1}, films with the EW in the range of 42 252 to 889 g eq^{-1} were produced. The fully ionized sample has nominally EW = 1000 g eq^{-1}; however, as indicated by the product data sheet, the measured EW may be lower than the nominal EW value. The equivalent weight of the membranes was determined by acid–base titration using the relation EW = m/Mv; where m is the dry mass of the sample recorded after acidification treatment; M is the solution molarity; and v is the titrated volume. The membranes in the H^+ form were placed in a 1 M NaCl solution for 30 min and the proton concentration back titrated with a 0.01 M NaOH solution, standardized with potassium biphtalate.

2.2.3. Nafion membranes prepared by electric and magnetic field-assisted casting. Commercial Nafion 5% solutions were evaporated and the polymer residue was redissolved in DMSO. The nanostructured Nafion films (MagCast) were prepared by pouring Nafion/DMSO solution into a Teflon casting mold containing a built-in SmCo magnet (bottom) with a second

SmCo magnet (upper) placed parallel to a metallic support, 15 mm from the base magnet. With a gaussmeter, the magnetic field of 0.5 T was measured in this arrangement. Nafion membranes preparation by electric field (ElecCast) was done in a Teflon casting mold containing a built-in parallel stainless steel plates by applying a dc electric field of 9 V cm^{-1}. A reference casting membrane was prepared by pouring Nafion/DMSO solution in a stainless steel casting mold (Cast). The samples were prepared with the thickness ranging from 0.5–3 mm for cross sectional SAXS measurements. The casting was performed at 160 °C during 6 h. All the membranes were pre-treated by standard cleaning and activation protocols.[21] The obtained films were then post-treated in 3% (w/w) H_2O_2 and 0.5 M H_2SO_4, with intermediate steps in H_2O to remove excess chemicals. For converting the membranes into the Cs^+ form, membranes were immersed in 0.5 M CsCl solution at room temperature for 10 h to ensure the complete exchange of H^+ by Cs^+.

The water uptake (WU) was calculated as the ratio between the mass of the absorbed water and the mass of dry polymer using the following equation:

$$\mathrm{WU}\% = \frac{M_\mathrm{w} - M_\mathrm{D}}{M_\mathrm{D}} \times 100, \quad (1)$$

where M_w is the mass of wet polymer and M_D is the mass of the dry polymer. The dry mass was obtained by placing the samples in a vacuum oven for 3 h at room temperature. The wet mass was obtained by immersing the samples in water for 3 h at room temperature. Prior to the mass acquisition, the membranes were blotted dry with a filter paper. The same approach was applied to estimate the percentage of thickness expansion of the prepared materials. The thickness was measured using a millesimal micrometer. Temperature dependent thickness expansion was also measured. For these measurements, the samples were placed in a resistive furnace for 2 h in the temperature range of 80 to 200 °C with incremental steps of 10 °C. Eqn (1) was used to estimate the percentage of thickness expansion upon annealing.

2.3. SAXS and WAXS

The SAXS/WAXS measurements were combined to evaluate the degree of ordering in the crystalline and amorphous phases, as well as to obtain the characteristic shape of the ionic and non-ionic phases of the ionomers prepared by all methods. The samples were examined by SAXS/WAXS at the beam line BM26-B[30] at the European Synchrotron Radiation Facility (ESRF) in Grenoble, France. The energy of X-ray source was 12 keV (λ = 0.1033 nm), and sample to detector distance in SAXS/WAXS was 3005/278 mm respectively. Data was recorded using the Pilatus 1 M/300k detector, with 172 × 172 μm pixel size. SAXS measurements were performed in longer timeframes in order to detect eventual X-ray beam damages, the data are shown in Fig. S1 of the ESI.†[60] The X-ray exposure time of the experiments was 10 s. The samples were heated at 2 °C min^{-1} from 20 °C to 250 °C, cooled at 40 °C min^{-1} to 20 °C, heated again at 2 °C min^{-1} to 300 °C and finally cooled at 10 °C min^{-1} to 20 °C, in a Linkam DSC600 hot stage for the simultaneous SAXS temperature-dependent study. The SAXS/WAXS patterns were reduced by BUBBLE and by the homemade XRTools software. The scattering Intensity (I) *vs.* scattering vector, $q = 4\pi \sin\theta\lambda^{-1}$, where λ is the X-ray wavelength and 2θ is the scattering angle. The scattering vector was calibrated using silver behenate and α-Al_2O_3. The scattering patterns were also corrected for transmission, normalized upon primary beam fluctuations and background scattering before data integration. The TFE crystallite sizes in Nafion were estimated using Scherrer equation in the WAXS plots. The degree of crystallinity was obtained by deconvolving the crystalline peak from the amorphous halo. The percentage of crystallinity is estimated by the ratio of the area under the crystalline peak and the convolved total area.

2.4. FTIR (mid and far infrared)

The FTIR measurements both in the mid and far ranges were combined to evaluate the role of the electrostatic interactions in the phase formation and stabilization. Specifically, the far infrared also permits obtaining information regarding the polarization of charges across the length scales of the building blocks, which is related to the data obtained by SAXS.[31,32] Variable temperature MIR and FIR spectra were measured at the IRIS beamline at the electron storage ring BESSY II of Helmholtz Zentrum Berlin (HZB).[31] FIR and MIR were measured in transmission mode through an in-vacuum operating Harrick FTIR Cell using the internal source for the mid infrared and infrared synchrotron radiation in spectral region between 600 and 30 cm^{-1} in the Bruker Vertex 70/v using a DLaTGS (MIR) and a liquid helium cooled silicon bolometer (FIR) detectors. The spectra were taken at 2 cm^{-1} resolution with 32 scans co-added. The references were taken through the empty channel inside the spectrometer sample compartment under vacuum. Prior to the measurements, the membranes were preconditioned in the Harrick cell by purging N_2 (relative humidity, RH, of 0.1%) for 24 h at room T. The relative humidity was recorded using a humidity sensor (Sensiriont EK-H4) at the outlet of the cell. The data collection was performed on N211 and N115 samples in the 30–200 °C T-range with a step of 10 degrees in two successive heatings. Measurements were performed after ~10 min at each temperature for system stabilization, when no noticeable spectral changes were observed.

2.5. AFM

AFM experiments were carried out on an Agilent AFM/SPM Series 5500 microscope in ACAFM contact mode, and in JEOL scanning probe microscope in the tapping mode. A sharp silicon beam-deflection cantilever was used. Observations were conducted on multiple areas to confirm both the uniformity and the reproducibility of the encountered experimental conditions. The topology images were measure in the back and forward scanning directions, at 0 and 90° to separate the real sample features from artifacts. AFM topology images were obtained at 25 °C.

2.6. Electrochemical characterization: proton conductivity and fuel cell tests

The acquisition of electrical spectra in the impedance and dielectric permittivity representations provides detailed information

on the motion and accumulation of charges across the ionomer phase separation, and allows matching the structural/electrostatic properties with the sample physical properties. The electrical understanding provides, in turn, the main factors associated with the overall electric performance in fuel cells.

Impedance/dielectric spectroscopy measurements were performed using a parallel-plate sample-holder made of stainless steel (through-plane). The proton conductivity measurements were performed from room temperature up to 80 °C at RH = 100%. The through-plane measurements were performed on the samples sandwiched with carbon-cloth contacts for improving electrical contact between sample and the sample-holder as well as allowing the diffusion of water molecules through the membrane for equilibrating with the relative humidity (RH = 100%) of the conductivity chamber.[21] The frequency response analyzer Solartron 1260 was used for carrying out the experiments in the frequency (f) range of 4 mHz to 3 MHz applying an ac amplitude of 100 mV.[21] The complex conductivity ($\sigma^* = 2\pi f \varepsilon_0 \varepsilon^*$) and dielectric permittivity ($\varepsilon^* = \varepsilon' - i\varepsilon''$) representations were used throughout this study, in which the dielectric spectra were obtained from:

$$\varepsilon^*(f) = \frac{1}{M^*(f)} = -\frac{S}{2\pi f \varepsilon_0 d Z^*(f)}, \quad (2)$$

where ε' and ε'' are the real and imaginary parts of the dielectric permittivity; ε_0 is the vacuum permittivity ($\sim 8.854 \times 10^{-14}$ F cm^{-1}); S is the electrode active area, d is the thickness of the membrane; $|Z|$ and θ are the modulus and phase angle of impedance respectively. Conductivity measurements were performed in duplicates.

Electrically and magnetically structured Nafion films were evaluated in a 5 cm^2 single fuel cell. Fuel cell tests were performed using Evaluator-C (FuelCon® AG). The electrode membrane assembly (MEA) was prepared by cold pressing the prepared Nafion films with a carbon cloth painted catalyst ink. The hot-pressing is known to promote morphology transitions of the ionomer phase, and therefore it was avoided. The catalyst ink composition was prepared with 0.4 mg Pt cm^{-2} (Pt/C catalyst – BASF) loadings at both anode and cathode. The thicknesses of the hydrated membranes were ~220 μm and ~245 μm, for N117, ElecCast and Magcast, respectively. The fuel cell was fed with pure hydrogen and oxygen at ambient pressure, 80 and 130 °C and RH = 100%. The polarization curves were obtained in duplicate experiments with estimated error of ~10% after 2 h to reach the stationary state. In the proof-of-concept fuel cell experiments, the MagCast fuel cell performance was obtained in duplicates (Fig. S9, ESI†).

2.7. Optical characterization: UV-visible spectroscopy

The charge polarization by the nanophase separation is intimately associated with the sample optical properties, which is identified by the different colors the samples prepared by electric and magnetic fields possess. UV/Vis absorption spectra were recorded by an Ocean Optics CCD spectrophotometer with fiber optics at BESSYII (HZB). UV/Vis spectra were collected over 1 ms with averaging of 16 UV/Vis spectra to improve the signal to noise ratio.

3. Results and discussion

3.1. Ordering of the non-ionic domains of Nafion: variable temperature SAXS, WAXS and FTIR

In the state-of-the-art interpretation of Nafion SAXS plots, the matrix peak is attributed to the scattering of the long range period among lamellar TFE crystallites.[1] The increase in crystallinity due to annealing is reported to increase the matrix peak intensity due to a higher number of scattering centers and a higher degree of ordering.[1] However, a careful inspection of the SAXS, WAXS and FTIR data of Nafion (1100 g eq^{-1}) performed as a function of temperature, as observed in Fig. 2, shows exactly the opposite trend. Initially, the SAXS/WAXS features in favour of the current interpretation will be addressed, and posteriorly, the main evidences against such assignments will be confronted.

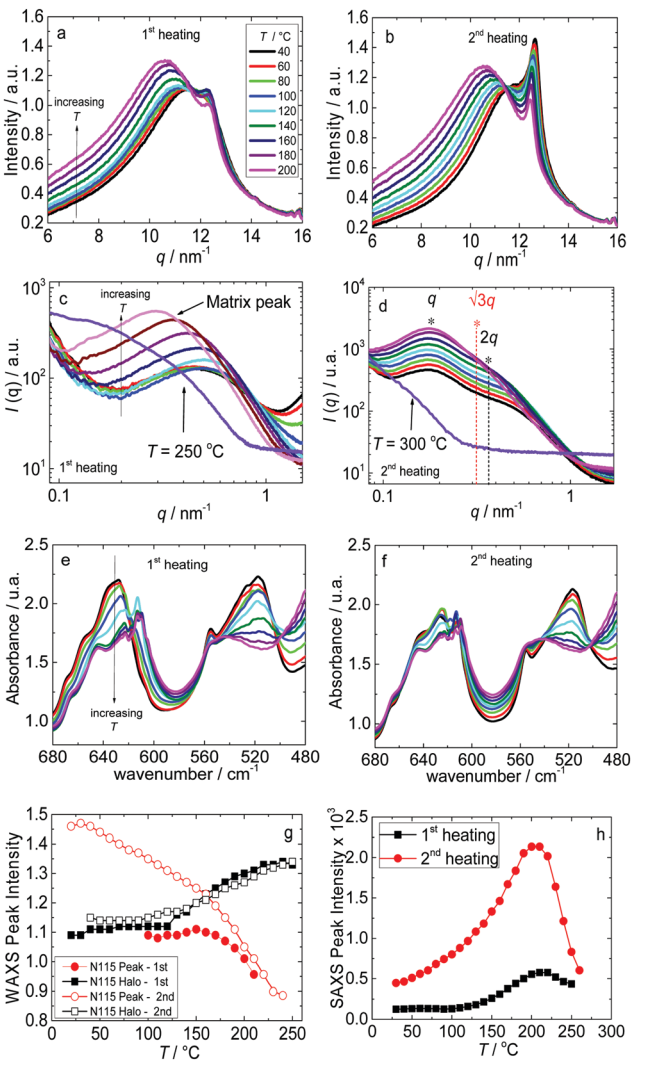

Fig. 2 Variable temperature WAXS (a and b), SAXS (c and d) and FTIR (e and f) plots for Nafion in the first and second heatings using the synchrotron sources from the ESRF and IRIS beamlines, respectively; (g) shows the amorphous halo and crystalline peak intensities, and (h) shows the matrix peak intensity as a function of temperature.

In the WAXS plots of Fig. 2a, the peak due to the crystalline phase in the 1st heating at $q \sim 12.0\ nm^{-1}$ (at 40 °C) is observed. By comparing Fig. 2a and b, it is observed that the crystalline peak displays a higher intensity and is displaced to high-q in the 2nd heating ($q \sim 12.5\ nm^{-1}$ at 40 °C), confirming that annealing promotes a higher degree of crystallinity as well as a higher degree of ordering of the crystalline phase. In addition, by comparing the 1st and 2nd heatings, at 120 °C, the crystallite size increases from 7.5 to 12.3 nm and the degree of crystallinity increases from 3.8 to 7.2%, respectively. Similarly, in the SAXS plots of Fig. 2c and d, a higher matrix peak intensity and a shift to lower q ($q \sim 0.14\ nm^{-1}$ at 40 °C) are observed in the 2nd heating compared to the 1st heating ($q \sim 0.46\ nm^{-1}$ at 40 °C). Considering previous models, such an increase in intensity of the matrix peak is usually attributed to the increase of the number of crystallites and the low-q displacement to an increase of their correlation distance from $d \sim 13.6$ to 44.9 nm.[3] All these aspects of the SAXS and WAXS plots are in accordance with the current assignment of the matrix and ionomer peaks of Nafion.[1]

However, in the temperature range of 40–250 °C in the 1st heating the matrix peak in the SAXS plots (Fig. 2c) exhibit the evolution of a single peak to double convoluted scattering, as can be seen in the indicated SAXS plot at 250 °C. Such bimodal scattering can be better visualized in the 2nd heating in SAXS plots of Fig. 2d. According to the current state-of-the-art interpretation, the single-to-double evolution would indicate an increased ordering of the crystalline phase with increasing T; however in this study this is contradicted by both, the reduction of ordering and degree of crystallinity with increasing T (in the same T-range). In both heatings (Fig. 2a and b), the crystalline peak intensity decreases with increasing temperature. Specifically, in the 2nd heating (Fig. 2b), the degree of crystallinity decreases from 8.1 to 4.6% in the 40–250 °C T-range. Moreover, as indicated by the low-q shift of the matrix peak in SAXS plots with increasing T (Fig. 2c), the increase of the correlation length from $d \sim 13.6$ to 44.9 nm, of the annealed membrane, which would indicate the presence of larger crystallites, cannot be accounted for by the reduction of the crystallite size observed by WAXS.

The reduction of the degree of crystallinity in the 1st and 2nd heatings can also be attested in temperature dependent FTIR measurements shown in Fig. 2e and f. Information concerning the changes of the degree of crystallinity of Nafion samples based on the wagging and rocking bands of CF_2 groups can be seen in the 700–500 cm^{-1} spectral range.[33,34] It has been previously observed that the 520 cm^{-1} band in polytetrafluoroethylene, assigned to CF_2 wagging, decreases in intensity with increasing temperature up to its total disappearance at the melting point.[33,34] Fig. 2e and f shows that with increasing T, the 520 cm^{-1} band disappears at 200 °C, as a result of the TFE crystals' melting. The reduction of the crystallinity as inferred from the 520 cm^{-1} band takes place in both heatings, which is in excellent agreement with the reduction of crystallinity discussed in WAXS analysis.

Interestingly, Fig. 2h shows that the matrix peak decreases in intensity for $T > 205$ °C due to the melting of the crystalline phase, evidencing that indeed there is a contribution of the crystallites to the intensity of the matrix peak. However, Fig. 2g shows that the intensity of the amorphous halo increases and is shifted to lower q-values with increasing T in both heatings, which matches the increase of the matrix peak intensity with increasing T in the same range (Fig. 2d). Therefore, the matrix peak intensity displays both contributions of the scattering of the crystalline and amorphous phases. Despite the contribution of the crystalline phase to the matrix peak intensity, the profile of the SAXS curve, *i.e.*, the double reflections in both heatings, suggests that the matrix peak represents the long-range periodic structure of the amorphous phase, in which the phase contrast is reinforced by the presence of high density crystallites.

In Fig. 3, the effect of thermal annealing on the structural rearrangement of Nafion morphology is schematized based on the new assignment of the matrix peak. As Nafion membrane is a copolymer with a non-uniform distribution of main and side

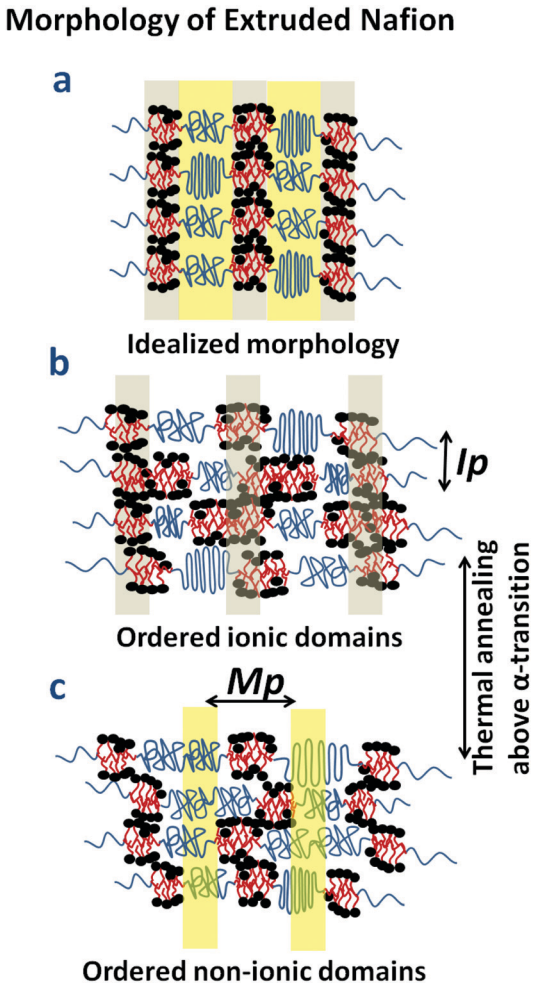

Fig. 3 Scheme of the coupling between ordering–disordering of both ionic and non-ionic domains above α-transition: (a) shows an idealized morphology for the case when Nafion is a perfect block copolymer; (b) shows the structure of as-received Nafion; and (c) the loss of correlation of ionic domains with thermal annealing followed by the rearrangement of the non-ionic phase in as-received Nafion membrane. Mp and Ip stands for matrix peak and ionomer peak, respectively.

chains along the polymer backbone, and the ionic network is formed in a matrix with an existing phase separation between main and side chains, its representative structure deviates from that observed for idealized phase separation (Fig. 3a). The grey and yellow shades in Fig. 3 represent the periodicity of the ionic and non-ionic domains, respectively.

At lower temperatures, up to 120 °C, the SAXS plots display an intense ionomer peak, which disappears for higher T.[32] Fig. 3b shows the ordering of the ionic domains, while the non-ionic domains have low degree of correlation; a situation that gets reversed above the α-transition temperature (Fig. 3c). For $T > 120$ °C, the increase in intensity of the matrix peak is an indication of an enhanced phase separation and correlation of the non-ionic domains. From the Fig. 3, the reinforcement of the matrix peak with increasing the degree of crystallinity can be better understood. The higher crystalline/amorphous ratio is, the higher is the scattering contrast between ionic and non-ionic domains. Such a scheme suggests that the irreversibility of the morphology in the 2nd heating is a result of the correlation existing among the non-ionic phase; and gives a further insight of how different shapes are memorized for such ionomers.

Therefore, Fig. 2g and h evidence an interplay between the disordering of the sulfonic group clusterings and the ordering of the amorphous non-ionic phase. This type of restructuring has been previously observed in other copolymer materials, and the single-to-double peaks transition was reported to originate from the contrast existing between ionic and non-ionic amorphous phases and represents a shape transition of the non-ionic domains.[35] It is worth noting that the presence of large crystallite sizes obtained in the second heating ($d \sim 12$ nm) indicates that at least a sequence of scarce side chain segments of 94 TFE units exists along the polymer backbone thereby suggesting an even more concentrated distribution of the monomer and comonomer in Nafion, in accordance with previous simulation studies of Nafion membranes.[9]

Based on the similarity to the high-order packing of block copolymers, the transition of single-to-double peaks in Nafion SAXS data can be explained by considering the long sequences of ionic and non-ionic monomeric distribution.[35] The most commonly arrangements for block copolymers morphologies are the lamellar and cylindrical packing of ionic and non-ionic phases.[35] Both morphologies exhibit multiple reflections in the SAXS plots with the respective sequences: q^*, $2q^*$, $3q^*$, *etc.* for lamellar, and q^*, $\sqrt{3}q^*$, $2q^*$, $\sqrt{7}q^*$, *etc.* for cylindrical packing.[35] In Fig. 2d, as can be seen at the indicated reflections in the SAXS plot, due to the high convolution between the SAXS reflections and the absence of a peak, it becomes difficult to discern the onset of the second reflection. However, previous reports showed that the lamellar or cylindrical reflections can be better identified in Kratky plots.[35,36] The Kratky plot of annealed Nafion (2nd heating) shown in the Fig. S4 of ESI,† confirms that the presence of q^* and $2q^*$ in the SAXS plots of annealed Nafion. In the SAXS plots of non-annealed Nafion, the single matrix peak observed at room temperature and humidity is very broad indicating a more disordered phase separation of the non-ionic phase. In addition, from the AFM phase image of Nafion (Fig. S5, ESI†) can be deduced that the shape of the non-ionic aggregates is nearly fibrillar, suggesting that the annealing treatment promotes a transition from disordered cylindrical structure to a lamellar arrangement of the non-ionic phase. As such, the matrix peak represents the correlation distance ($d \sim 10$ nm) among the packed fibrillar non-ionic aggregates for non-annealed Nafion.

3.2. Ordering of the ionic phase of Nafion: equivalent weight dependence of morphology

By controlling the relative fractions of the monomer and comonomer, the supramolecular electrostatic interactions among functional groups allow for self-assembling of a diverse number of structures.[35] Such approach can be used to provide further insights into the trade-off between the ordering of the ionic and non-ionic phases.

The stability of each shape is dependent on the fraction of the comonomer as well as the thermodynamics of the phase incompatibility.[35] The EW was varied within the range from 42 252 to 889 g eq^{-1}. Samples in the SO_3Cs were also studied since these groups have a higher tendency of aggregation due to the higher dipolar attraction. The ionomer and matrix peaks and the electrostatic interactions as a function of EW were studied by SAXS, MIR and FIR spectroscopy, respectively, as shown in Fig. 4.

It is worth noting that for the samples with a low degree of crystallinity, in X-ray diffraction experiments, the amorphous

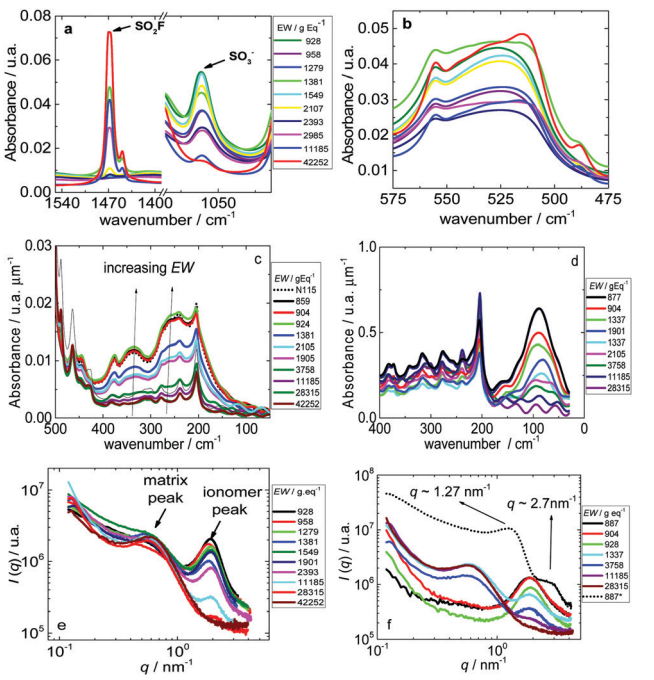

Fig. 4 MIR (a and b) plots as a function of EW (from 42 252 to 889 g eq^{-1}) for Nafion in the H^+ form; FIR (c and d) and SAXS (e and f) and plots as a function of EW (from 42 252 to 889 g eq^{-1}) for Nafion in the H^+ and Cs^+ forms using the synchrotron source from the IRIS beamline, respectively. The dotted curve in (b) is the SAXS plot for Nafion-Cs^+ in the wet form.

halo superposes the crystalline peak of Nafion, as can be observed in Fig. 2a, inhibiting the study of the effect of the degree of crystallinity with the changes in EW.

Fig. 4a and b show the FTIR spectra for Nafion in the fingerprint region evidencing the increase of the sulfonic acid groups band with decreasing EW and the corresponding changes in the spectral features associated with the crystallinity, respectively. It can be seen in Fig. 4a that as the EW decreases, the band at 1065 cm^{-1}, associated with the SO_2 stretching in SO^{3-} group, increases, and the band associated with the SO_2 vibrations in SO_2F, decreases. In Fig. 4b, it is observed that the relative intensity of the 520 cm^{-1} band (CF_2 wagging) with respect to the 555 cm^{-1} band (CF_2 bending) of the samples prepared by hot-pressing followed by quenching, is significantly reduced ($wCF_2/bCF_2 \sim 1.1$) as compared to the ones observed in Fig. 2e for commercial extruded Nafion ($wCF_2/bCF_2 \sim 1.3$). Moreover, the wCF_2 band shift to higher frequencies is reported for PTFE with decreasing crystallinity.[33,34] In Fig. 4b, the wCF_2 band is observed at 526 cm^{-1}, whereas in Fig. 2e, it is observed at 516 cm^{-1} confirming a lower degree of crystallinity in the membranes prepared by hot-pressing as compared to the extruded ones. This feature confirms that the liquid N_2 quenching allowed producing samples with a low degree of crystallinity. In addition, no noticeable changes in the relative intensity of wCF_2/bCF_2 were observed in Fig. 4b for the samples with increasing EW. For example, the wCF_2/bCF_2 for EW of 42 252 and 928 g eq^{-1} are 1.15 and 1.12, respectively. Nonetheless, the appearance of the 555 cm^{-1} band in the spectrum of samples with high EW (42 252, 11 185 and 2985 g eq^{-1}) indicates the existence of ordered crystalline domains, which is suppressed for EW $<$ 2985 g eq^{-1}.[34] This feature indicates that the reduction of the degree of crystallinity takes place with increasing EW. However, the SAXS matrix peaks for Nafion both prepared by hot-pressing and extrusion are centered at $q \sim 0.5$ nm^{-1}, indicating that there is no association between the degree of crystallinity and the correlation distance indicated by the matrix peak. Similarly to the assignment of the matrix peak made in Fig. 2, the matrix peak studied as a function of EW reinforces the interpretation that the matrix peak represents the correlation distance within the non-ionic phase that contains both amorphous and crystalline TFE phases.

The ionic clustering is confirmed by FIR (Fig. 4c and d), as inferred from the appearance of the cation motion bands for Nafion in the H^+ (240 and 335 cm^{-1}) and Cs^+ (97 cm^{-1}) forms.[31,37] The cation motion band of ionomers is related to the ion polarization across the length scales of the ionic aggregates of the sample. With increasing of the ionic content by decreasing EW, a random conversion of the ionic sites along the ionomer matrix would be expected. Therefore, with decreasing EW, the formation of the ionic aggregates takes place, possibly resulting in the increase in the intensity of the cation motion band, as it is observed in Fig. 4c and d. However, the existence of the cation motion band at very low EW ($\sim$11 185–28 315 g eq^{-1}) is an evidence that possibly there are ionic aggregates at incipient ionic conversion. Such aggregation is confirmed by the presence of the stretching of SO_3H bands due to hydrogen bonding in the MIR range (not shown).

The formation of ionic aggregates at very low EW is confirmed in the SAXS plots (Fig. 4e and f). However, the ionomer peak in SAXS plots has the same position in all EW samples studied. Unlike the theory of ionic aggregation in ionomers in which the increase of the ionic content increases the size of the ionic clusters, the similar size of the ionic aggregates regardless of sample EW can be possibly understood by considering an already existing phase separation of the non-ionic copolymer that acts as template for the formation of ionic clusters.[38,39] Previous AFM measurements of Nafion-SO_2F revealed that even in the non-ionic form Nafion topology displays a phase separation in the nanometric range.[39] As a template, the distance among the ionic domains is determined by the non-ionic phase separation of the precursor matrix. The ionic conversion decorates gradually the segments of Nafion rich in side chain terminated functional groups, by the $SO_2F \rightarrow SO_3H$ conversion, giving rise to the ionomer peak position insensitive to EW. This ionomer peak behavior has been also observed for SEBS.[38] The SAXS data as a function of EW shown for Nafion in Fig. 4e and f are in accordance with the matrix peak assignment made in Fig. 2. In the non-ionic form, Nafion SAXS plots display only the matrix peak at $q \sim 0.6$ nm^{-1} (Fig. 4e and f), and the gradual ionic conversion promotes an increase of the ionomer peak intensity and a broadening of the matrix peak.

In the Cs^+ form (Fig. 4f), the reduction of the matrix peak with decreasing EW is even more pronounced and the matrix peak is suppressed for EW $<$ 1337 g eq^{-1}. The increased relative intensity of the ionomer peak with respect to the matrix peak for Cs^+ neutralized Nafion membranes is a result of a higher electron contrast existing between ionic and non-ionic phases, which may be an outcome of two factors: (i) the higher valency of Cs^+ counterions compared to the H^+ form;[40] and (ii) the electrostatic attraction among sulfonate groups for Nafion is stronger in the neutralized form also providing a high degree of packing of the ionic phase.[40] Both factors are possibly associated with the differences between Nafion-H^+ and Nafion-Cs^+ SAXS patterns. Previous SANS measurements confirmed that a higher ordering of the ionic domains exists for Nafion in the Cs^+ form as compared to the H^+ form.[40] However, the most relevant feature is the SAXS patterns of Nafion-Cs^+ in the hydrated state as shown in Fig. 4f. In the hydrated form, the ionomer peak of Nafion-Cs^+ is displaced to lower q-values ($q^* \sim 1.27$ nm^{-1}) revealing a new reflection for the ionomer peak at $q \sim 2.70$ nm^{-1} (nearly $2q^*$) (Fig. 4f). In the ESI,† the SAXS plots of Nafion in the humid and in the cesium form (Fig. S2, ESI†) are shown with decreasing EW confirming the existence of the double-reflections for the ionomer peak. This measurement shows that the double-reflections observed for the ionomer peak are not due to the form factor undulations.

Similarly, such disorder-order interplay between ionic and non-ionic domains is commonly observed in sulfonated styrene-ethylene/butylene-styrene copolymers (SEBS).[38] SEBS copolymers in the non-ionic form exhibit the hexagonal packing of the polymeric aggregates, as evidenced by characteristic SAXS reflections.[38] The ionic clustering due to sulfonation of SEBS gives rise to the ionomer peak at high-q, resembling the SAXS plot of Nafion.

With decreasing EW, the strong electrostatic interactions among the sulfonate groups in Nafion samples decrease the ordering (matrix peak) of the polymeric aggregates. Therefore, the SAXS study of Nafion with increasing both T and EW provides compelling evidences that the ionomer and matrix peaks are due to ordering of both amorphous ionic and non-ionic phases, respectively. It also provides evidence for a preferential ordering of a lamellar ionic phase with respect to the non-ionic one due to enthalpic contributions of the ionic supramolecular interactions among SO_3H and SO_3Cs.

3.3. Ordering of the ionomer peak of Nafion: application of electric and magnetic fields

The application of an electric and magnetic potential are known to promote an alignment of copolymer morphology by dielectric polarizability and magnetic susceptibility, respectively.[41,42] In ionomers, this is rather enhanced due to the presence of ionic domains. Therefore, such alignment and ordering of the ionic phase could provide an unequivocal identification of the lamellar reflections of the ionic phase of Nafion. Fig. 5a–c show the SAXS and azimuthal plots of Nafion prepared by electric (ElecCast) and magnetic field-assisted casting (MagCast). Fig. 5d shows the 2D SAXS patterns revealing the anisotropic orientation of the ionomer peak, and Fig. 5e shows a schematic representation of the lamellar arrangement of the side chains.

Fig. 5a shows that the ionomer peaks of MagCast and ElecCast, as measured with the X-ray beam positioned perpendicularly to the membrane surface, are similar to the ones observed by the sample prepared by casting (Cast), indicating no noticeable ordering of the ionic domains along the membrane surface. On the other hand, Fig. 5b shows the SAXS plots of Nafion prepared by ElecCast and MagCast measured with the X-ray beam parallel to the membrane surface, in which a marked increase in intensity and narrowing of the ionomer peak is observed. Moreover, the higher order reflection can be clearly identified at $q \sim 3.76$ nm^{-1} confirming that the ionomer peak of Nafion exhibits the characteristic lamellar reflections ($q^* \sim 1.88$ nm^{-1}/$2q^* \sim 3.76$ nm^{-1}) of phase separation for both ElecCast and MagCast.

Fig. 5d shows that the observed anisotropic 2D patterns are very similar to the ones observed in mechanically stretched Nafion films.[1] In such stretched samples, the ionomer peak was observed to decrease in intensity in the meridional direction (stretching direction), while an increase in intensity was observed in the equatorial direction (transversal to drawing direction).[1,4,5] The 2D SAXS plots of electrically and magnetically aligned Nafion show an increase in intensity of the ionomer peak in the meridional direction and a suppression of the ionomer peak in the equatorial direction. The anisotropy of the ionomer peaks of MagCast and ElecCast can be better visualized in the azimuthal plots of Fig. 5c. In Fig. 5c, the ionomer peaks are more strongly anisotropic for MagCast compared to the plots of ElecCast, indicating a higher degree of ordering of the ionic phase due to the magnetic field.

In accordance to the SAXS patterns, the lamellar packing of the ionic and non-ionic domains is schematically represented in Fig. 5e. The lamellar ordering of ionic aggregates has already been postulated for Nafion membranes.[6,8,43–45] Two distinct lamella stacking possibilities were previously proposed for Nafion.[13,46] In one of them, the main chain folding of a crystalline TFE lattice into a hairpin conformation with the side chains pointing outward the crystallite folding forming a lamellar bilayered structure was suggested.[46] Two aspects of the

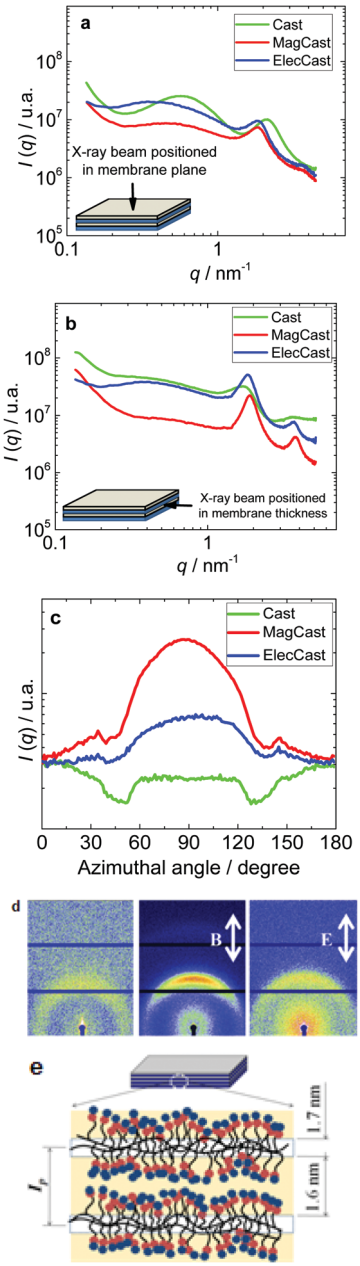

Fig. 5 SAXS plots for Nafion membranes prepared by electric and magnetic field-assisted casting measured with the X-ray beam in perpendicular (a) and parallel (b) to the membrane surface. In (c), the azimuthal plots of the ionomer peak for the membranes prepared by electric and magnetic-assisted casting are shown. In (d), the 2D SAXS plots evidencing the anisotropic scattering of the samples; B and E stand for the magnetic and electric field directions, respectively. In (e), a schematic representation of the lamellar arrangement of the ionic domains is presented.

ionomer peak observed in Fig. 5 point to such hairpin lamellar ordering as improbable for Nafion: (i) in the hairpin arrangement, the side chains must be regularly distributed along the polymer backbone since they cannot be accommodated into the crystallites;[46] and (ii) considering the crystallite size (~3–12 nm) and the approximate side chain length (~0.8 nm) the lamellae thickness would be much larger, *ca.* ~4.6 to 13.6 nm, compared to the estimated values from Fig. 4b (~3.3 nm). An alternative arrangement previously suggested for copolymers with perfluorinated side chains[47] was where the lamellar correlation length associated with the ionomer peak corresponds to twice the average length of the side chains. This arrangement of the side chains for Nafion was already proposed by Starkweather *et al.*[13] If the side chains are in a head-to-tail configuration all the side chains would be located at the same side of the main chain.[13]

In this way, a lamella is formed when two side chains are placed side-by-side with the side chains forming the bilayered structure, as shown in Fig. 5e. The resulting lamellar thickness in this model (~2.6 nm) is a sum of the width of two fluorocarbon chains (~1 nm),[13] and twice each side chain length ($2L$ ~ 1.6 nm). Such lamellar packing is a typical feature observed in fluorinated side-chain smectic copolymers—comb-shaped polymers with fluorocarbon segments in their sidechains.[47,48] It is important to notice that in this arrangement the nonuniform monomeric distribution is permitted and the estimated lamellar thickness is in much closer agreement with experiment. The divergence between the measured lamellar thickness (~3.3 nm) and those estimated by considering the dimensions of Nafion main and side chains (~2.6 nm) is possibly a result of residual water content, which increases the lamellar spacing.

Since transmission electron microscopy promotes a high rate of degradation of the ionomer, atomic force microscopy (AFM) has been constantly used to estimate the size and shape of the polymer phases in a broad range of length scales.[14] Fig. 6 shows the AFM images of the electrically and magnetically aligned Nafion membrane and the images of Nafion prepared by casting for comparison. Fig. 6a–c show the topography images of the Cast, ElecCast and MagCast alongside with the corresponding 3D topographies.

The phase images of the topography and the topology height profile for the indicated arrows in Fig. 6 are shown in Fig. S6 (ESI†) respectively. Fig. 6a shows in the image an isotropic arrangement with a 50 nm sized domains, which were previously assigned to the aggregation of bunches of ~10 nm sized cylindrical polymeric aggregates.[49] Fig. 6c displays a 5 × 5 μm^2 topology window of Nafion revealing a stacked lamella perpendicularly oriented with the applied magnetic field direction in excellent agreement with the SAXS plots of Fig. 5. The 3D topology (Fig. 6c) and phase image (Fig. S6, ESI†) views reveal the lamella terraces aligned parallel to the membrane plane with a long period ranging from 3 to 12 nm (Fig. S7, ESI†). Both alignment and the lamella correlation length evidence that the topology features observed by AFM matches perfectly the ionomer peak in the SAXS plots. Likewise for MagCast, the ElecCast

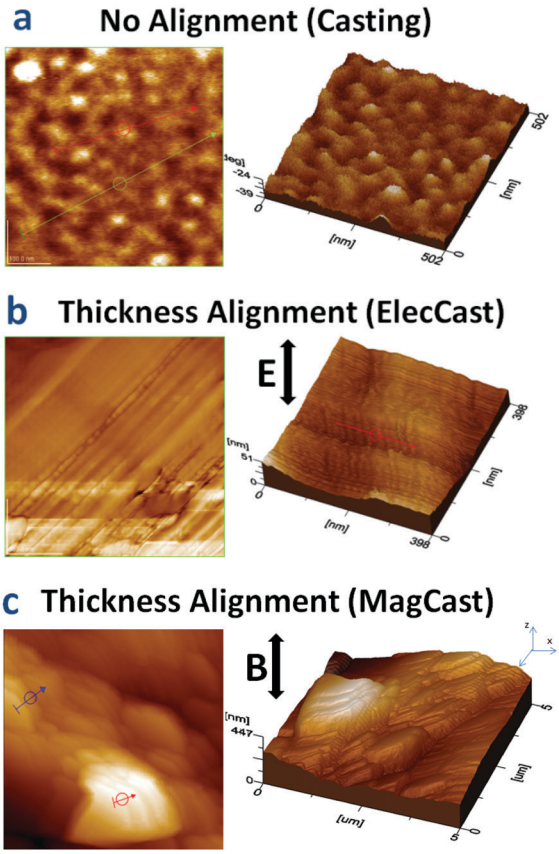

Fig. 6 AFM topography images alongside with the corresponding 3D topography plot of pristine cast Nafion (a), ElecCast (b) and MagCast (c).

membrane (Fig. 6b) exhibits a characteristic lamellar structure with a characteristic average steps ranging from ~3 to 10 nm thickness (Fig. S6, ESI†). The lamella in ElecCast is ordered in a similar arrangement compared to MagCast, however, the lamellas are inclined with respect to the membrane surface, which can be associated with different orientations for the lamella and consequently, to the lower ordering found for the sample modified by electric field (Fig. 6b). It is worth of note that the phase image of Fig. 6b for ElecCast (Fig. S6, ESI†) evidences underlying features of the membrane morphology. It can be observed in Fig. S6 (ESI†) the presence of elongated nearly cylindrical aggregates with radius and length of ~12 and 130 nm, respectively, which composes the internal structure of the lamellar phase.

In order to gain a further insight into the internal arrangement of the lamellar structure observed in Fig. 6, higher magnification of the topologies of the lamellar phase are shown in Fig. 7. It can be seen from Fig. 7 that the building blocks of the morphology of both MagCast and ElecCast are polymeric aggregates with an approximate diameter and length of ~10 and 100 nm, respectively. These dimensions of the polymeric aggregates are in accordance with recent reports on Nafion dispersions in solvents of low dielectric constant, which revealed polymeric aggregates with a radius of gyration of ~100 nm.[50] Moreover, the ~10 nm diameter of the polymeric aggregates is in good agreement with the correlation length estimated by the matrix peak in Fig. 4a of

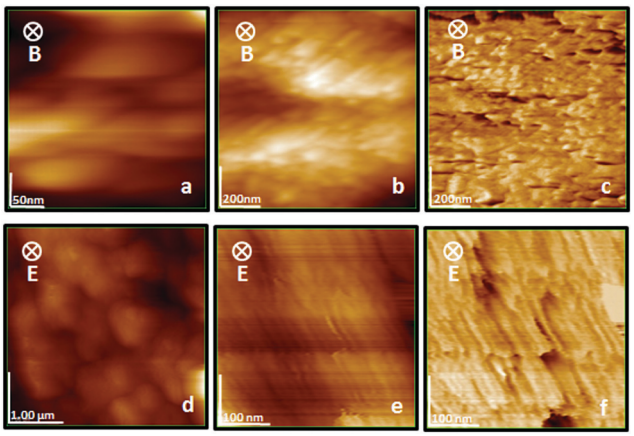

Fig. 7 AFM topography images (a and b) and phase image (c) of the magnetically aligned Nafion film. AFM topography images (d and e) and phase image (f) of the electrically aligned Nafion film.

~13 nm, indicating that the cylindrical aggregates are due to the non-ionic aggregates core that are lined with the lamellar arrangement of the ionic domains. In Fig. 7a–c, it can be seen that the cylindrical polymeric aggregates are positioned with a preferential orientation parallel to the magnetic field vector. Such orientational order is commonly observed in magnetically aligned copolymers and mainly arises due to the alignment along the highest rotational symmetry by the anisotropy in magnetic susceptibility.[41,42] On the other hand, the ElecCast building blocks are aligned in the direction perpendicular to the electric field vector. Such feature indicates that the electric alignment produces a similar anisotropy to the extruded Nafion films shown in Fig. 6b. The combination of the results obtained by SAXS and AFM indicate that the lamellar ionic domains are oriented in the same direction for both ElecCast and MagCast and that the non-ionic domains are oriented in opposing orthogonal direction.

In Fig. 5b, by comparing the SAXS plots of ElecCast and MagCast in the thickness and plane directions, it can be seen that there is an intense scattering upturn for $q < 0.3$ nm^{-1} only in the thickness direction for MagCast, which is absent for ElecCast. Such large intensity at low q is associated with the length of the polymeric aggregates.[3] This feature is in accordance with the cylindrical alignment along the membrane thickness shown in AFM images for ElecCast and MagCast. For the anisotropic alignment of the nonionic aggregates shown in Fig. 7c for MagCast, the scattering associated with the length of the polymeric aggregates would be present in SAXS plots only positioning the beam in the membrane thickness (Fig. 5b).

The water sorption of ElecCast and MagCast membranes are in accordance with the percentage of membrane expansion due to water sorption. Cast, ElecCast and MagCast membranes display the water sorption of 30%, 34% and 41%, whereas the thickness expansion are 13%, 20% and 27%, respectively, confirming that the water sorption is preferentially due to the lamellar expansion along the thickness direction of the membrane,[58] as detected by AFM. According to previous reports, even the cast membranes display a lamellar arrangement of the ionic domains.[6] In this scenario, the increasing water uptake of the Cast, ElecCast and MagCast follows the sequence of increasing degree of ordering of the ionic domains as measured by SAXS. The misalignment of the stacked lamella may restrict the polymer expansion and, consequently, the water sorption capacity. In Fig. S8 (ESI†), a higher degree of expansion is found in the thickness direction for the pristine Cast samples, compared to the low thickness dependence on temperature for ElecCast and MagCast. Similarly, the higher ordering of the lamellar phase enhances the compactness of the ionic domains resulting in a smaller thickness expansion with increasing temperature.

3.4. Dielectric/Impedance spectroscopy and the electric/magnetic alignment mechanism

In Fig. 8, the real and imaginary components of the proton conductivity (Fig. 8a) and the dielectric permittivity (Fig. 8b) spectra, respectively, for Nafion at $T = 40$ °C and RH = 100% are shown. According to the AFM measurements shown in Fig. 6 and 7, the rotational axis of the elongated non-ionic domains are oriented in parallel to the membrane surface for extruded Nafion (Fig. S5, ESI†) and ElecCast (Fig. 7f), whereas in the magnetic-field cast membrane, the long axis of the non-ionic domains are perpendicularly oriented to the membrane surface (Fig. 7c). Fig. 8c shows the orientation of the non-ionic domains of ElecCast and MagCast as inferred from the AFM measurements of Fig. 7, showing how the ionic and non-ionic domains are further oriented in the through-plane conductivity/dielectric measurements. Considering such anisotropic arrangement, in the through-plane measurements shown in Fig. 8a, the protonic polarization of the radius and length of the non-ionic domains would only exist for the orientation displayed for extruded Nafion and ElecCast films. For MagCast, the radius of the nonionic domains does not offer additional polarization that would hinder the proton motion along the membrane thickness, as indicated in Fig. 8c. This result is in good agreement with the measurements shown in Fig. 8a. The dielectric loss of N117 and ElecCast membranes exhibit an additional polarization at $f \sim 10^2$ Hz compared to the MagCast curve. The relation $f^{-1} = L^2 6D^{-1}$, where D is the diffusion coefficient, allows estimating the correlation length (L) of the effective polarization, and the calculated value is $L \sim$ 10–30 nm, which supports the evidence that such polarization is due to the charge accumulation across the radius of the non-ionic domains.

As the extruded Nafion 117 and ElecCast exhibit the non-ionic polarization, the proton transport experiences a higher tortuosity, thereby reducing the proton conductivity, as can be seen in Fig. 8b. The real spectra of Nafion proton conductivity displays a high ($f > 10^5$ Hz) and low ($f < 10^{-1}$ Hz) frequency plateaus, assigned to the proton conductivity in aqueous media and across the polymer heterogeneities (dc conductivity), respectively.[51,52] In MagCast samples, both proton conductivities are increased due to the absence of the extra polarization of the non-ionic domains, which increases the mean free path for proton transport. Specifically at low frequencies an improvement of the dc proton conductivity of one order of magnitude is observed for MagCast ($\sigma \sim 3 \times 10^{-7}$ S cm^{-1}) compared to the one observed for N117 ($\sigma \sim 8 \times 10^{-8}$ S cm^{-1}) and ElecCast

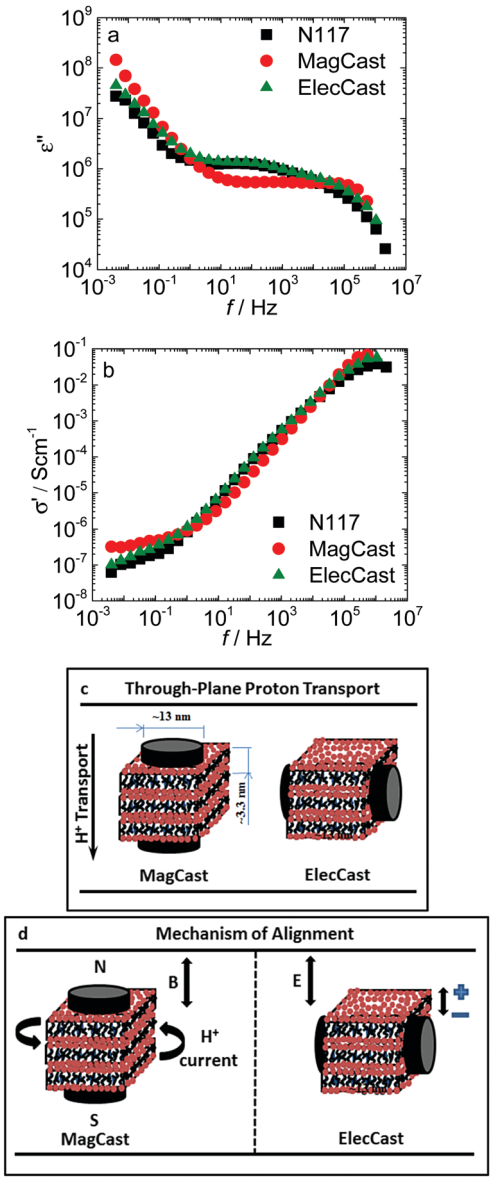

Fig. 8 Imaginary part of the dielectric permittivity (a) and the real part of the conductivity (b) for Nafion at 40 °C and RH = 100% measured in the through-plane setup. In (c) the schematic representation of the lamellar stacking of ionic and nonionic domains, indicating the matrix (in black) and ionomer (in red) peaks are shown. In (d), the mechanisms of the alignment of the ionomer building blocks in solution are schematized.

($\sigma \sim 9 \times 10^{-8}$ S cm^{-1}), at T = 40 °C and RH = 100%. The dielectric and conductivity spectra are in good match with the SAXS/AFM structural anisotropy identified for Cast, ElecCast and MagCast, which provides important insights into the polarization mechanism of the ionomer building blocks, helping to distinguish such systems of high polarizability with the traditional mechanism of alignment found in block copolymers. As previously reported, Nafion exhibits colossal dielectric permittivity values,[53,54] which can be easily identified in the dielectric spectra of Fig. 8a. For all the samples, the dielectric loss values are in the $\sim 10^6$ units in the frequency range of $f \sim 10^1$–10^6 Hz (Fig. 7a). Dielectric constant is basically dependent on the dipole moment of macromolecules, as in polyethylene, and on the number of orienting dipoles existing in the polymer, as in polyvinyl chloride.[51] However, for both systems, the values of dielectric permittivity loss of polyethylene and polyvinyl chloride are usually below 10 units.[51] The huge dielectric permittivity values, such as the ones observed for Nafion, are found in polyelectrolytes, where there is a high linear charge density of ionic groups exceeding the Bjerrum length limit, which promotes the counterion condensation into the polymer chains, *i.e.*, the counterions exhibit a higher degree of coordination with the anionic compensation site (sulfonic groups).

According to Freeman-Manning approach,[15,23] such counterions are in constant fluctuation and polarize the length scales of the polymer building blocks (Fig. 8c), which in turn are understood as microdipoles. This phenomenon is possibly the central mechanism linked to the high degree of ordering of Nafion ionic domains using such modest electric and magnetic fields. For the ElecCast membranes, the application of the electric field in Nafion solution promotes the polarization of the ionic phase of the nearly cylindrical aggregates shown in Fig. 8d, resulting in the alignment of the lamellar thickness in perpendicular direction with the through-plane electric field of the casting mold. For MagCast membranes, the looping diffusion of condensed counterions within the ionic phase that surrounds the non-ionic cylindrical core, as seen in Fig. 8d, produces a magnetic field along the rotational axis of the polymeric aggregates, which align along the through-plane magnetic field of the casting mold.

3.5. Physical properties of the nanostructured Nafion: electrochemical and optical properties

Fig. 9 shows the H_2/O_2 fuel cell tests for the nanostructured membranes at T = 80 °C and RH = 100% (Fig. S8 of the ESI,† shows the duplicate fuel cell tests).

The dc proton conductivity at low frequencies (Fig. 8b) represents the influence of the long-range polymer structure in the proton transport. Fig. 9 shows an enhancement of the PEM performance by using the magnetically nanostructured Nafion films, and a poor PEM performance for ElecCast. The linear fit of the ohmic drop region of the IV-curve provides the specific resistances ~1.19 and 0.65 Ohm cm^2 for N117 and MagCast Nafion films evidencing that the specific resistance of magnetically structured films is halved in PEMs, in very good agreement with the proton conductivity data.

Compared to the state-of-the-art polarization curves, the N117 fuel cell performance observed in Fig. 9 is lower. Previous N117 fuel cell reports showed that at T = 70 °C and RH = 100%, the fuel cell current density is 600 mA cm^{-2} (at 400 mV).[55] Similarly, it was observed that at T = 80 °C and RH = 100%, the current density at 500 mV is 600 mA cm^{-2}.[56] In our measurements, the N117 fuel cell current density at 400 mV is 230 mA cm^{-2}. This is mainly because we have not performed the usual hot pressing (~130 °C) in the membrane electrode assembly. It is worth emphasizing that the MEAs were prepared without hot-pressing in order to avoid morphological changes of the samples due to thermal annealing. However, at ~400 mV the current density of PEM using MagCast is significantly improved

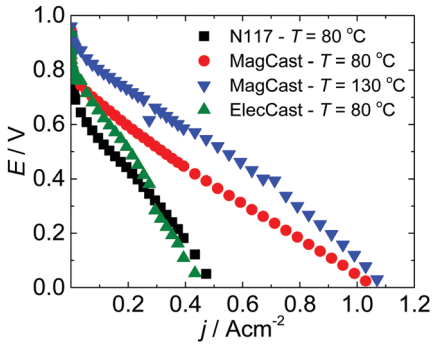

Fig. 9 H_2/O_2 polarization curve for unmodified Nafion and the electrically and magnetically aligned Nafion membrane at T = 80 °C and RH = 100% (c).

from ~230 to 500 mA cm^{-2}. With increasing T from 80 to 130 °C, the fuel cell performance is further improved to 650 mA cm^{-2} (at ~400 mV), indicating that MagCast membranes are promising for high temperature PEM.

Although ElecCast displays poorer performance in fuel cells, ElecCast displays distinguished optical properties, as can be seen by the color green of such materials in the Fig. S10 (ESI†). In order to evaluate the optical properties of the films FIR and UV-Vis spectroscopy measurements are shown in Fig. 10a and b, respectively.

Fig. 10a evidences new absorption bands for ElecCast at 322 and 100 cm^{-1} that can be related to the ion polarization across new length scales existing though the modification of Nafion by the electric field. The periodic multi-layer dielectric stacking

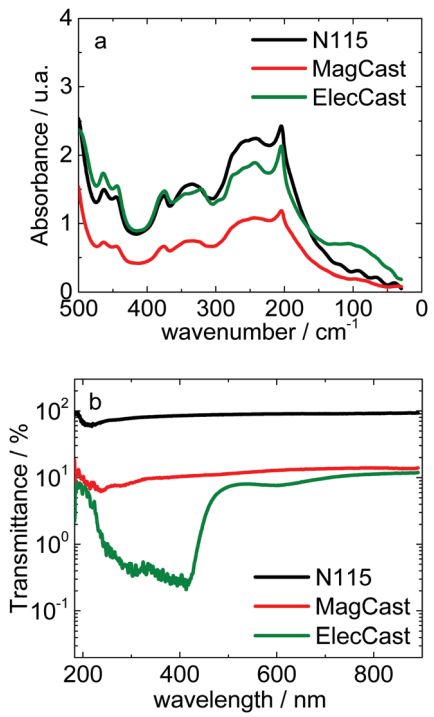

Fig. 10 (a) FIR and (b) UV-visible spectroscopy of Nafion 115, ElecCast and MagCast.

structure of ElecCast conferred to such material photonic crystal properties.[57] The properties of polymeric photonic crystals are related to the lamellar size and refractive index contrast of the nanophase separation. Fig. 10b shows that ElecCast displays an intense absorption in the 200–400 nm wavelength range, and a weak absorption at ~610 nm, and both absorptions are associated with the film green color. Interestingly, both ElecCast and MagCast display a high degree of absorbance compared to transparent Nafion, which could lead to a higher performance in photovoltaic cells.[57]

As such, the liability of Nafion under the influence of electric and magnetic fields, associated with the proton transport and optical properties could find new applications in which Nafion films have not been previously considered, such as electric-driven displays, electrochromic coloring materials, and solar cells.

4. Conclusions

In summary, the SAXS/WAXS and FTIR analyses in a broad range of temperature and equivalent weight indicate that the matrix peak of Nafion SAXS plots is due to the separation of amorphous/crystalline TFE nonionic domains with an average period of ~10 nm. Moreover, the combination of SAXS/WAXS and FTIR for high-temperature annealed Nafion evidenced the presence of higher crystallinity and domains of higher ionic density, suggesting a monomeric sequence of Nafion backbone with a higher degree of blockiness in two alternate segments of the ionic and non-ionic monomers—one TFE rich segment, and another side chain rich segment—than it was previously reported. The SAXS analysis of Nafion quenched in liquid nitrogen (low crystallinity) in the caesium form evidenced a higher ordering of the ionic domains due to stronger electrostatic attractions revealing lamellar reflections of the ionomer peak. Both the thermal annealing and equivalent weight studies suggest that the most representative chemical structure of Nafion is the random or statistical block copolymer. The enhanced lamellar ordering of the ionic domains were found for electrically and magnetically structured Nafion films prepared by casting, as revealed by SAXS and AFM studies. However, the samples prepared by electric and magnetic fields display different orientations of the non-ionic domains. The mechanism for the alignment of the ionic domains is distinct for the electric and magnetic field-assisted casting in which the existence of condensed counterions in Nafion plays a key role in the charge polarization process, resulting in high degree of polarizability and a high ability to promote the alignment of Nafion building blocks under low intensity electric and magnetic fields. The nanostructured Nafion films by electric and magnetic fields displayed enhanced electrochemical and optical properties. The parallel orientation of the non-ionic domains with respect to the proton transport for magnetically aligned Nafion resulted in a minimization of the charge polarization across the non-ionic domains, increasing the mean free path for proton transport. The perpendicular orientation of the non-ionic domains with respect to the proton

transport direction in extruded Nafion and the electrically aligned Nafion resulted in an increased tortuosity for proton migration. Accordingly, the sample prepared by magnetic field exhibited higher proton conductivity and elevated fuel cell performance at low and high temperature experiments. The magnetic induced ordering of perfluorinated ionomer membranes is a promising method for controlling the anisotropic conductivity and enhancing PEM performance. In contrast, the nanostructured films prepared with electric field-assisted casting displays properties of photonic crystals, making them promising materials for solar cells.

Conflicts of interest

There are no conflicts to declare.

Acknowledgements

Thanks are due to J. F. Q. Rey and D. Hermida-Merino (SAXS and WAXS). We thank the ESRF, the HZB and the LNLS (20160239) for the allocation of synchrotron radiation beamtime. Authors are grateful for the support of the Center for Innovation on New Energies CINE – SHELL (ANP)/FAPESP (17/11937-4), the Research Center for Gas Innovation RCGI – SHELL (ANP)/FAPESP (14/50279-4) and the Comissão Nacional de Energia Nuclear (CNEN). FCF is a fellow of the Brazilian CNPq (305620/2019-3). Thanks are also due to the funding supports FAPESP 2014/09087-4 and 2013/50151-5.

References

1 A. Kusoglu and A. Z. Weber, New Insights into Perfluorinated Sulfonic-Acid Ionomers, *Chem. Rev.*, 2017, **117**, 987–1104.
2 K. Schmidt-Rohr and Q. Chen, Parallel cylindrical water nanochannels in Nafion fuel-cell membranes, *Nat. Mater.*, 2008, **7**, 75–83.
3 X. Linga, M. Bonna, K. F. Domkea and S. H. Parekh, Correlated interfacial water transport and proton conductivity in perfluorosulfonic acid membranes, *Proc. Natl. Acad. Sci. U. S. A.*, 2019, **116**, 8715–8872.
4 P. C. van der Heijden, L. Rubatat and O. Diat, Orientation of Drawn Nafion at Molecular and Mesoscopic Scales, *Macromolecules*, 2004, **37**, 5327–5336.
5 L. Rubatat, A. L. Rollet, G. Gebel and O. Diat, Evidence of Elongated Polymeric Aggregates in Nafion, *Macromolecules*, 2002, **35**, 4050–4055.
6 K. D. Kreuer and G. Portale, A Critical Revision of the NanoMorphology of Proton Conducting Ionomers and Polyelectrolytes for Fuel Cell Applications, *Adv. Funct. Mater.*, 2013, **23**, 5390–5397.
7 F. I. Allen, L. R. Comolli, A. Kusoglu, M. A. Modestino, A. M. Minor and A. Z. Weber, Morphology of Hydrated as-Cast Nafion Revealed through Cryo Electron Tomography, *ACS Macro Lett.*, 2015, **4**, 1–5.
8 S. Lyonnard, Q. Berrod, B.-A. Bruning, G. Gebel, A. Guillermo, H. Ftouni, J. Ollivier and B. Frick, Perfluorinated surfactants as model charged systems for understanding the effect of confinement on proton transport and water mobility in fuel cell membranes. A study by QENS, *Eur. Phys. J. Special Topics*, 2010, **189**, 205–216.
9 S. S. Jang, V. Molinero, T. Çağın and W. A. Goddard, Nanophase-Segregation and Transport in Nafion 117 from Molecular Dynamics Simulations: Effect of Monomeric Sequence, *J. Phys. Chem. B*, 2004, **108**, 3149–3157.
10 E. A. Weiber, D. Meis and P. Jannasch, Anion conducting multiblock poly(arylene ether sulfone)s containing hydrophilic segments densely functionalized with quaternary ammonium groups, *Polym. Chem.*, 2015, **6**, 1986–1996.
11 D. Chen and M. A. Hickner, Ion Clustering in Quaternary Ammonium Functionalized Benzylmethyl Containing Poly(arylene ether ketone)s, *Macromolecules*, 2013, **46**, 9270–9278.
12 E. A. Weiber and P. Jannasch, Ion Distribution in Quaternary-Ammonium-Functionalized Aromatic Polymers: Effects on the Ionic Clustering and Conductivity of Anion-Exchange Membranes, *ChemSusChem*, 2014, **7**, 2621–2630.
13 H. W. Starkweather Jr, Crystallinity in perfluorosulfonic acid ionomers and related polymers, *Macromolecules*, 1982, **15**, 320–323.
14 R. Koestner, Y. Roiter, I. Kozhinova and S. Minko, AFM Imaging of Adsorbed Nafion Polymer on Mica and Graphite at Molecular Level, *Langmuir*, 2011, **27**, 10157–10166.
15 G. S. Manning, Condensation of Counterions Gives Rise to Contraction Transitions in a One-Dimensional Polyelectrolyte Gel, *Polymers*, 2018, **10**, 432.
16 K. M. Beers, D. T. Hallinan Jr., X. Wang, J. A. Pople and N. P. Balsara, Counterion Condensation in Nafion, *Macromolecules*, 2011, **44**, 8866.
17 D. B. Spry and M. D. Fayer, Proton Transfer and Proton Concentrations in Protonated Nafion Fuel Cell Membranes, *J. Phys. Chem. B*, 2009, **113**, 10210.
18 Q. Chen and K. Schmidt-Rohr, 19F and 13C NMR Signal Assignment and Analysis in a Perfluorinated Ionomer (Nafion) by Two-Dimensional Solid-State NMR, *Macromolecules*, 2004, **37**, 5995–6003.
19 Q. Chen and K. Schmidt-Rohr, Backbone Dynamics of the Nafion Ionomer Studied by 19F-13C Solid-State NMR, *Macromol. Chem. Phys.*, 2007, **208**, 2189–2203.
20 G. Meresi, Y. Wang, A. Bandis, P. T. Inglefield, A. A. Jones and W.-Y. Wen, Morphology of dry and swollen perfluorosulfonate ionomer by fluorine-19 MAS, NMR and xenon-129 NMR, *Polymer*, 2001, **42**, 6153.
21 B. R. Matos, E. I. Santiago, J. F. Q. Rey and F. C. Fonseca, Origin of α and β relaxations of Nafion, *Phys. Rev. E: Stat., Nonlinear, Soft Matter Phys.*, 2014, **89**, 052601.
22 A. Münchinger and K.-D. Kreuer, Selective ion transport through hydrated cation and anion exchange membranes I. The effect of specific interactions, *J. Membr. Sci.*, 2019, **592**, 117372.
23 J. Peng and T. A. Zawodzinski, Describing ion exchange membrane-electrolyte interactions for high electrolyte

concentrations used in electrochemical reactors, *J. Membr. Sci.*, 2020, **593**, 117340.
24 M. Ghelichi and M. H. Eikerling, Conformational Properties of Comb-Like Polyelectrolytes: A Coarse-Grained MD Study, *J. Phys. Chem. B*, 2016, **120**, 2859–2867.
25 M. M. Hasani-Sadrabadi, F. S. Majedi, G. Coullerez, E. Dashtimoghadam, J. J. VanDersarl, A. Bertsch, H. K. Moaddel, I. Jacob and P. Renaud, Magnetically Aligned Nanodomains: Application in High-Performance Ion Conductive Membranes, *ACS Appl. Mater. Interfaces*, 2014, **6**, 7099–7107.
26 X. Liu, Y. Li, J. Xue, W. Zhu, J. Zhang, Y. Yin, Y. Qin, K. Jiao, Q. Du, B. Cheng, X. Zhuang, J. Li and M. D. Guiver, Magnetic field alignment of stable proton conducting channels in an electrolyte membrane, *Nat. Commun.*, 2019, **10**, 842.
27 H.-L. Lin, T. L. Yu and F.-H. Han, A Method for Improving Ionic Conductivity of Nafion Membranes and its Application to PEMFC, *J. Polym. Res.*, 2006, **13**, 379–385.
28 S. Ryu, J.-H. Kim, J.-Y. Lee and S.-H. Moon, Investigation of the effects of electric fields on the nanostructure of Nafion and its proton conductivity, *J. Mater. Chem. A*, 2018, **6**, 20836–20843.
29 Y. Wang, J. Gao, T. J. Dingemans and L. A. Madsen, Molecular Alignment and Ion Transport in Rigid Rod Polyelectrolyte Solutions, *Macromolecules*, 2014, **47**, 2984–2992.
30 G. Portale, D. Cavallo, G. C. Alfonso, D. Hermida-Merino and M. Van Drongelen, Polymer crystallization studies under processing-relevant conditions at the SAXS/WAXS DUBBLE beamline at the ESRF, *J. Appl. Crystallogr.*, 2013, **46**, 1681–1689.
31 L. Puskar, E. Ritter, U. Schade, M. Yandrasits, S. J. Hamrock, M. Schaberg and E. F. Aziz, Infrared dynamics study of thermally treated perfluoroimide acid proton exchange membranes, *Phys. Chem. Chem. Phys.*, 2017, **19**, 626–635.
32 B. R. Matos, R. Politano, J. F. Q. Rey, D. Hermida-Merino, U. Schade, L. Puskar and F. C. Fonseca, Interplay of α/β-Relaxation Dynamics and the Shape of Ionomer Building Blocks, *Sci. Rep.*, 2018, **8**, 13441.
33 R. G. Brown, Vibrational Spectra of Polytetrafluoroethylene: Effects of Temperature and Pressure, *J. Chem. Phys.*, 1964, **40**, 2900.
34 H. W. Starkweather Jr., R. C. Ferguson, D. B. Chase and J. M. Minor, Infrared Spectra of Amorphous and Crystalline Poly(tetrafluoroethylene), *Macromolecules*, 1985, **18**, 1684–1686.
35 H.-K. Kwon, V. E. Lopez, R. L. Davis, S. Y. Kim, A. B. Burns and R. A. Register, Polystyrene-poly(2-ethylhexylmethacrylate) block copolymers: synthesis, bulk phase behavior, and thin film structure, *Polymer*, 2014, **55**, 2059–2067.
36 A. Ianiro, M. Chia, M. M. R. M. Hendrix, A. V. Koça, E. D. Erena, M. Sztuckic, A. V. Petukhovd, G. de With, A. C. C. Esteves and R. Tuinier, Block copolymer hierarchical structures from the interplay of multiple assembly pathways, *Polym. Chem.*, 2020, **11**, 2305–2311.
37 S. D. Bernardina, J.-B. Brubach, Q. Berrod, A. Guillermo, P. Judeinstein, P. Roy and S. Lyonnard, Mechanism of Ionization, Hydration, and Intermolecular H-Bonding in Proton Conducting Nanostructured Ionomers, *J. Phys. Chem. C*, 2014, **118**, 25468–25479.
38 J. Kim, B. Kim and B. Jung, Proton conductivities and methanol permeabilities of membranes made from partially sulfonated polystyrene-*block*-poly(ethylene-ran-butylene)-*block*-polystyrene copolymers, *J. Membr. Sci.*, 2002, **207**, 129–137.
39 R. S. McLean, M. Doyle and B. B. Sauer, High-Resolution Imaging of Ionic Domains and Crystal Morphology in Ionomers Using AFM Techniques, *Macromolecules*, 2000, **33**, 6541–6550.
40 M. A. Dresch, B. R. Matos, F. C. Fonseca, E. I. Santiago, M. Carmo, A. J. C. Lanfredi and S. Balog, Small-angle X-ray and neutron scattering study of Nafion-SiO_2 hybrid membranes prepared in different solvent media, *J. Power Sources*, 2015, **274**, 560–567.
41 P. W. Majewski, M. Gopinadhan, W.-S. Jang, J. L. Lutkenhaus and C. O. Osuji, Anisotropic Ionic Conductivity in Block Copolymer Membranes by Magnetic Field Alignment, *J. Am. Chem. Soc.*, 2010, **132**, 17516–17522.
42 Y. Rokhlenko, M. Gopinadhan, C. O. Osuji, K. Zhang, C. S. O'Hern, S. R. Larson, P. Gopalan, P. W. Majewski and K. G. Yager, Magnetic Alignment of Block Copolymer Microdomains by Intrinsic Chain Anisotropy, *Phys. Rev. Lett.*, 2015, **115**, 258302.
43 S. Shen, A. Han, X. Yan, J. Chen, X. Cheng and J. Zhang, Influence of Equivalent Weight of Ionomer on Proton Conduction Behavior in Fuel Cell Catalyst Layers, *J. Electrochem. Soc.*, 2019, **166**, F724–F728.
44 D. I. Kushner, A. Kusoglu, N. J. Podraza and M. A. Hickner, Substrate-Dependent Molecular and Nanostructural Orientation of Nafion Thin Films, *Adv. Funct. Mater.*, 2019, 1902699.
45 H.-G. Haubold, T. Vad, H. Jungbluth and P. Hiller, Nano structure of NAFION: a SAXS study, *Electrochim. Acta*, 2001, **46**, 1559–1563.
46 M. H. Litt, A Reevaluation of Nation Morphology, *Polym. Prepr.*, 1997, **38**, 80.
47 G. de Crevoisier, P. Fabre, L. Leibler, S. Tencé-Girault and J. M. Corpart, Structure of Fluorinated Side-Chain Smectic Copolymers: Role of the Copolymerization Statistics, *Macromolecules*, 2002, **35**, 3880–3888.
48 J.-M. Corpart, S. Girault and D. Juhue, Structure and Surface Properties of Liquid Crystalline Fluoroalkyl Polyacrylates: Role of the Spacer, *Langmuir*, 2001, **17**, 7237–7244.
49 A. Lehmani, S. Durand-Vidal and P. Turq, Surface Morphology of Nafion 117 Membrane by Tapping Mode Atomic Force Microscope, *J. Appl. Polym. Sci.*, 1998, **68**, 503–508.
50 J. H. Lee, G. Doo, S. H. Kwon, S. Choi, H.-T. Kim and S. G. Lee, *Dispersion-Solvent Control of Ionomer Aggregation in a Polymer Electrolyte Membrane Fuel Cell*, Sci. Rep., 2018, **8**, 10739.
51 A. Schönhals and F. Kremer, in *Broadband Dielectric Spectroscopy*, ed. F. Kremer and A. Schönhals, Springer Verlag, Berlin, 2003, p. 59.
52 B. R. Matos, E. I. Santiago, J. F. Q. Rey, C. H. Scuracchio, G. L. Mantovani, L. A. Hirano and F. C. Fonseca, *dc* Proton

conductivity at low-frequency in Nafion conductivity spectrum probed by time-resolved SAXS measurements and impedance spectroscopy, *J. Polym. Sci., Part B: Polym. Phys.*, 2015, **53**, 822–828.

53 S. J. Osborn, M. K. Hassan, G. M. Divoux, D. W. Rhoades, K. A. Mauritz and R. B. Moore, Glass Transition Temperature of Perfluorosulfonic Acid Ionomers, *Macromolecules*, 2007, **40**, 3886–3890.

54 J.-H. Lin and R. H. Colby, Evolution of morphology, segmental dynamics, and conductivity in ionic liquid swollen short side chain perfluorosulfonate ionomer membranes, *J. Polym. Sci., Part B: Polym. Phys.*, 2015, **53**, 1273–1280.

55 X.-Z. Yuan, S. Zhang, H. Wang, J. Wu, J. C. Sun, R. Hiesgen, K. A. Friedrich, M. Schulze and A. Haug, Degradation of a polymer exchange membrane fuel cell stack with Nafion® membranes of different thicknesses: Part I. In situ diagnosis, *J. Power Sources*, 2010, **195**, 7594–7599.

56 E. Proietti, F. Jaouen, M. Lefèvre, N. Larouche, J. Tian, J. Herranz and J.-P. Dodelet, Iron-based cathode catalyst with enhanced power density in polymer electrolyte membrane fuel cells, *Nat. Commun.*, 2011, **2**, 416.

57 Y. Huang, Y. Zheng, J. Pribyl and B. C. Benicewicz, A Versatile Approach to Different Colored Photonic Films Generated from Block Copolymers and Their Conversion into Polymer-Grafted Nanoplatelets, *J. Mater. Chem. C*, 2017, **5**, 9873–9878.

58 M. J. Park, K. H. Downing, A. Jackson, E. D. Gomez, A. M. Minor, D. Cookson, A. Z. Weber and N. P. Balsara, Increased Water Retention in Polymer Electrolyte Membranes at Elevated Temperatures Assisted by Capillary Condensation, *Nano Lett.*, 2007, **11**, 3547–3552.

59 A. V. Rebrov, A. N. Ozerin, D. I. Svergun, L. P. Bobrova and N. F. Bakeyev, Small Angle X-Ray Scatter Study of the Aggregation of Macromolecules of the Perfluorosulphonated Ionomer in Solution, *Polymer Science U.S.S.R.*, 1990, **32**, 1515–1521.

60 Y. Iwai, A. Hiroki, M. Tamada, K. Isobe and T. Yamanishi, Radiation deterioration of ion-exchange Nafion N117CS membranes, *Radiat. Phys. Chem.*, 2010, **79**, 46–51.